Solar RRL
www.solar-rrl.com

Pressure Effects on Lead-Free Metal Halide Perovskites: a Route to Design Optimized Materials for Photovoltaics

Marta Morana and Lorenzo Malavasi**

Metal halide perovskites have drawn significant attention for their promising physical properties and their possible application in solar cells and light-emitting diodes. Research and technology have made extraordinary progress in this field, but some issues are still to be tackled. In fact, most of the used materials contain lead, which is highly toxic. For this reason, many efforts have been made on substituting lead with other elements to design more environmentally friendly solar cells. However, devices based on lead-free materials still show relatively low efficiencies. Physical properties tuning of such materials, to improve their performance, can be achieved in different ways, and among them pressure can be thought of as a green method for this aim as well as a powerful technique to systematically explore structure–property relationships. The possibility of unveiling and discovering novel and appealing optical and electronic features, resulting from the application of an external pressure, can open an effective route to design more performing materials.

1. Introduction

Since hybrid perovskites were first proposed as visible light sensitizers for photovoltaic cells,[1] these materials have attracted an increasing amount of attention, leading to the design and characterization of a plethora of different compositions, structures, and devices.[2–5] The terms "hybrid perovskites" and "metal halide perovskites" encompass, not always properly,[6,7] different families of materials. The aristotype perovskite has stoichiometry ABX_3 and space group $Pm\bar{3}m$, as in the case of $SrTiO_3$, and is formed of corner-sharing BX_6 octahedra and a monovalent cation A, enclosed in a cubic cage. The so-called Goldsmith tolerance factor t can be used as a figure of merit to understand whether a perovskite structure can form: the ABX_3 structure is stable for t between 0.8 and 1.[8] In the case of hybrid perovskites, A is usually a small organic cation such as methylammonium (MA) or formamidinium (FA), B is a bivalent cation, and X is a halide. Octahedral tilting, the position of the organic cation, and how they interact with the inorganic framework then generate different configurations and space group symmetries.[9] In addition, the bivalent B cation can be replaced by one monovalent cation B and a trivalent cation B′ to form a so-called double perovskite of formula $A_2BB'X_6$.[10] In hybrid organic–inorganic metal halides when the size of the A organic cation increases, the compounds usually assume the A_2BX_4 stoichiometry and a structure comprising layers of BX_6 octahedra alternated with a layer of organic cations.[3] Also, a mixture of organic cations is used, a small A and a large L cation, giving raise to the stoichiometry $[L]A_{n-1}B_nX_{3n+1}$, where n is the number of octahedral layers.[3,4] These compounds are usually referred to as layered or 2D perovskites, in contrast with the ABX_3 considered a 3D perovskite.[2–4,7] When bulky cations are used, the resulting compounds are formed by single chain or completely isolated octahedra, usually called 1D or 0D perovskites, even if the use of the term "perovskite" for these cases is still debated.[7] Physical properties of metal halides are strongly affected by their structure. For example, the bandgaps are defined by the orbital overlap between the metal and the halide ions, in terms of the angular distortion between adjacent metal halide octahedra that can be quantified as the deviation from 180° of the B–X–B angle: a larger deviation corresponds to a wider bandgap.[11–15] On the contrary, the distortion within the octahedra is usually related to a broader photoluminescence (PL) emission.[16] The A cations have a more indirect influence on the bandgap, interacting through hydrogen bonds with the octahedral layers and affecting the B–X–B angle.[14] Understanding the relationship between the structure and the bandgap is of paramount importance because it is one of the parameters determining the solar spectrum absorption. In fact, the maximum theoretical efficiency of a solar cell using a single p–n junction, known as Shockley–Queisser limit, is 33.7% with a bandgap of 1.34 eV.[17,18] Tuning this parameter through chemical substitution or a thermodynamic variable such as pressure allows for the design of efficient devices.

1.1. Lead-Free Hybrid Organic–Inorganic Metal Halides

Metal halide perovskites have shown interesting properties and performances in solar cells, including the recent record power conversion efficiency (PCE) of 25.6% reported for $\alpha - FAPbI_3$.[19] However, the most used materials, both in research and applications, usually contain lead that is highly

M. Morana, L. Malavasi
Department of Chemistry
University of Pavia and INSTM
Via Taramelli 16, 27100 Pavia, Italy
E-mail: marta.morana@unipv.it; lorenzo.malavasi@unipv.it

The ORCID identification number(s) for the author(s) of this article can be found under https://doi.org/10.1002/solr.202100550.

DOI: 10.1002/solr.202100550

toxic.[20,21] Two main strategies have been developed to address this problem: reducing lead leakage[22,23] and designing lead-free materials.[5,24] Considering the importance of the electronic structure of Pb^{+2} in determining optical characteristics, such as narrow bandgap and long carrier diffusion length,[25] possible alternatives for lead are cations with a similar electronic structure such as Sn, Ge, Bi, Cu, In, and Sb. In the following sections, a brief overview of well-characterized lead-free materials will be given. A full and detailed description of the results of this very active field is beyond the scope of this work, thus the interested reader is referred to more extensive accounts of this topic[24,26–32]

1.1.1. Sn-Based Compounds

In analogy with lead-containing perovskites, $ASnX_3$ compounds have been synthesized with A = MA and FA or Cs.[33] These materials as well show promising properties, for example, in $ASnI_3$ the bandgap is 1.30, 1.40, and 1.30 eV, for MA, FA, and Cs, respectively.[34] The bandgap can be further tuned changing the halide or through alloying on the A site. In fact, the bandgap varies from 1.3 for I to 3.61 eV for Cl in $MASnX_3$ and allowed to design a cell with PCE 5.73%,[26] whereas $(FA)_{0.75}(MA)_{0.25}SnI_3$ perovskite was successfully used in cells with PCE up to 8.12%.[35] 2D Sn-perovskites have also drawn considerable attention due to their enhanced stability to humidity and temperature.[36,37] Whereas a plethora of different organic cations have been evaluated, from the BA[38] to large aromatic cations,[39] the effect of the halide is still poorly described because it has been systematically explored only for BZA_2SnX_4 (BZA = benzylammonium) with bandgaps of 1.7, 2.4, and 3.04 eV for I, Br, and Cl, respectively.[40] The main drawback of these layered structures is a slower charge transfer and thus a lower efficiency. This problem has been addressed growing the perovskite film perpendicular to the substrate and combining 3D and 2D structures[41,42]; the last approach has allowed to reach up to 12.4%.[43] The main limit to the application of Sn-based materials in solar cell is the instability of Sn^{2+} that easily oxides to Sn^{4+} in ambient atmosphere. Addition of additives, such as SnF_2, is a possible strategy to inhibit the oxidation of Sn^{2+} that has shown promising results.[44]

1.1.2. Ge-Based Compounds

Ge is another possible alternative to lead, being abundant and less toxic, but germanium-based perovskites have been so far poorly explored.[45] Various $AGeI_3$ compound with A = Cs and organic cations were synthesized and showed a peculiar trend with the bandgap changing from 1.6 to 2.8 eV with the cation dimensions, whereas in Pb-based compound the A cation has a small influence on the bandgap.[46] Cation mixing in both the A and B sites has been reported, analogously to other metal halide perovskites. Substituting MA with FA modulates the gap 1.98–2.26 eV,[47] and replacing Sn with Ge varies it from 1.3 to 1.9 eV.[48] In addition, a solar cell based on $CsSn_{0.5}Ge_{0.5}I_3$ showed a PCE of 7.11%,[49] and one on $FA_0.75MA_0.25Sn_{1-x}Ge_xI_3$ yields an efficiency of 4.48%.[50] A limited amount of 2D Ge perovskites has been reported. $BA_2MA_{n-1}Ge_nBr_{3n+1}$ series was synthesized starting from $MAGeBr_3$ and layering with BA, allowing tuning of the bandgap 2.85 to 2.98 eV.[51] The aromatic phenylethylammonium (PEA) cation gives a bandgap of 2.12 eV[52] while mixing of Ge with Sn varies the gap from 1.95 to 2.13 eV.[53] Recently, 2D A_2GeBr_4 compounds have been reported, with A = BZA, PEA, Br-PEA, F-PEA.[54] In these systems, the presence of the Ge atoms seems to induce a large distortion within the octahedra, but a slighter effect on the angle between the octahedra with respect to Sn- and Pb-based compounds.[54]

1.1.3. Other Lead Free-Materials for Photovoltaic Applications

Double perovskites were also evaluated as lead-free alternatives. $Cs_2AgBiBr_6$ and $Cs_2AgBiCl_6$ show a good stability to air,[10,55] but large and indirect bandgaps of 2.19 and 2.77 eV, respectively. To tune the bandgaps, Bi can be substituted with In or Sb, enabling a modulation of 0.41 eV,[56] and $Cs_2AgInCl_6$ shows a gap of 3.23 eV.[57] Solar cells based on these materials have PCE of 0.42% for Cs_2NaBiI_6,[58] and up to 2.84% for $Cs_2AgBiBr_6$.[59] Other compounds containing Sb and Bi, which do not always assume the perovskite structure, have been developed as alternative to lead-based materials. $MA_3Bi_2I_9$, $MA_3Bi_2Br_9$, and $MA_3Sb_2I_9$ have bandgaps of 1.94,[60] 2.1,[61] and 2.14 eV,[62] whereas the inorganic $Cs_3Bi_2I_9$ has a gap of 2.2 eV.[61] In general, these materials have a good resistance to air, but poor performance due to their large bandgaps.[63]

1.2. High Pressure

As a thermodynamic parameter, pressure allows to explore phase transitions and structure–properties relations, generating new phases, triggering chemical reactions, and new electronic phenomena, that would be inaccessible at room conditions. Since their development in the late 1950s,[64] diamond anvil cells (DAC) have become the most popular device in high-pressure studies. The DAC is based on a simple and elegant design, comprising two opposed diamond anvils that create a pressure chamber, enclosed in a metal gasket. In the simplest and most common devices, the thrust-generating mechanism is based on variable number of screws or an inflatable membrane.[65] The pressure chamber usually contains the sample, a pressure sensor such as ruby,[66,67] quartz[68,69] or a metal,[70] and a pressure transmitting medium (PTM) to ensure hydrostaticity.[71,72] As diamond has low absorption for X-rays and is almost transparent to visible, IR, and UV radiation, DACs can be used for in situ diffraction and spectroscopy experiments, allowing for atomic-level understanding. Thus, high pressure can be used as a postsynthesis treatment to tune material properties and performance. In the field of photovoltaic and hybrid materials, high-pressure studies were mostly conducted on lead halide perovskites for which some general trends have been identified and described.[73–81] The response to compression is mostly related to the inorganic framework, in terms of contractions of the metal halide bonds and tilting of the octahedra.[75,76,80] The shortening of the bonds increases the orbital overlap and narrows the bandgap, whereas the bending of the angle between the octahedra enlarges it.[75,76,80,82] As already pointed out, the effect of the A cation is less direct, but becomes more important when moving away from the ideal ABX_3 structure. For example, replacing the MA cation in $MAPbBr_3$ with the larger FA one increases the tolerance factor to 1.01, thus close to the stability limit of the perovskite structure, and affects the

mechanical properties of the inorganic framework, weakening it and increasing the Pb–Br bond length of 1%.[83] This effect is even more striking when moving to layered structures: layered materials show a large range of bulk moduli, K_0, suggesting that different cation and thus different strains can tune the properties of this kind of structures.[73,74,84] The difference in compressibilities of the inorganic and organic layers affects the pressure response of layered perovskites. In $BA_2(MA)Pb_2I_7$ two pressure regimes can be clearly identified, related to the different layers,[82] and $(PEA)_2PbI_4$ shows a large anisotropy in its response to compression due to the fact that the organic layers are much easier to deform.[85] This peculiar response to compression is also coupled with desirable properties such as broad energy tunability,[85] bandgap narrowing, and PL enhancement, partially retained upon decompression.[82] In the case of all-inorganic perovskites for photovoltaic applications, attention has been mostly focused on $CsPbX_3$ compounds.[86–89] Notably, both $CsPbCl_3$ and $CsPbBr_3$ undergo an isostructural phase transition at 2.1 and 1.2 GPa, respectively, as a result of the tilting of the PBX_6 octahedra,[86,89] whereas $CsPbI_3$ transforms from an orthorhombic to a monoclinic phase at 3.9 GPa.[88] The three compounds have slightly higher bulk moduli then hybrid perovskites, but are much more compressible than oxide perovskites.[86,88,89] It is also worth mentioning that first-principles calculations suggest that the degree of octahedral tilting in halide perovskites depends both on orbital interactions between the inorganic species and hydrogen bonding, with the former dominating in inorganic perovskites and the latter playing a critical role in hybrid perovskites.[90] In addition, retention of high-pressure tuned properties upon decompression is an important characteristic, already reported in some materials. Application of high pressure followed by heating and rapid quenching allows to obtain a material that shows good stability in air.[91] However, also full reversibility of pressure-induced change might be interesting for materials and applications that require transient changes in the electronic properties.

2. High-Pressure Characterization of Lead-Free Metal Halides

The high-pressure characterization of lead-free metal halides is still relatively limited to a restricted number of materials. These are shown in **Table 1** and will be discussed in the following paragraphs.

2.1. The ABX_3 Structure

Lead-free perovskites crystallizing in the ABX_3 structure were the first to be characterized at high pressure. $MASnI_3$ crystallizes in the aristotype space group $Pm\bar{3}m$, undergoes a first phase transition to the body-centered $Im\bar{3}$ at 0.5 GPa, and a second transition after 2.2 GPa to $Immm$, to finally become amorphous above 4 GPa.[92] The driving force of the transition was identified in a relief of strain in the Sn—I bond because of the displacement the iodine off the $< 100 >$ axis rather than to ordering of the organic cations, as it occurs with temperature.[92] Interestingly, in a recent study $MASnI_3$ was reported to crystallize in space group $P4mm$ at ambient conditions and to undergo a phase transition to $Pnma$ at 0.7 GPa.[84] Both space groups, $Pm\bar{3}m$ and the pseudocubic $P4mm$, have been used to describe the crystal structures of $MASnI_3$ at ambient conditions because the former better represents the average structure and the latter the local structure.[27,93] The sample was subject to two cycles of compression. During the first cycle, $MASnI_3$ becomes amorphous at about 3 GPa and recrystallizes upon pressure release in $Pm\bar{3}m$,[84] as shown in Fig**ure 1**. In the second compression process, no amorphization can be observed above 30 GP and the conductivity is threefold higher than the initial value.[84] The two reports calculate a bulk modulus of 12.6(7)[84] and 12.3 GPa,[92] thus describing a highly compressible material.

Changing the halide seems to affect the phase transition behavior. $MASnBr_3$ was reported to undergo a single transition at approximately 1.5 GPa from the cubic $Pm\bar{3}m$ phase to an orthorhombic phase.[94] The orthorhombic phase persists up to 9.0 GPa, suggesting a large resistance against amorphization with respect to the iodine counterpart, and the cubic phase is restored after pressure release.[94] The phase transition to the orthorhombic phase corresponds to a large redshift of 0.4 eV, followed by a blueshift of 0.3 eV in the absorption spectroscopy data, and to a PL signal enhanced at moderate pressure that vanishes at the transition point.[94] This behavior was investigated by density functional theory (DFT) calculations that suggest that the variation of the bandgap is controlled in the stability field of the cubic phase by the contraction of the Sn—Br bond length and then by hydrogen bonding between the framework and the disorder organic cations.[94] On the contrary, $MASnCl_3$ shows a transition from a monoclinic phase Pc to a triclinic phase $P1$ that starts at 1.0 GPa and is completed at 2.3 GPa, whereas the amorphization begins at 4.1 GPa.[95] The tilting and distortion of the $[SnCl_6]^{4-}$ octahedra are the driving force of the phase transition, as confirmed by Raman and IR spectroscopy.[95] The primary absorption edge shows a distinct redshift below 1.0 GPa, and the bandgap varies from 3.61 eV at room conditions to 3.33 eV at 3.0 GPa (**Figure 2**). The transition is fully reversible.[95]

Different organic cations also affect the response to pressure of tin halide hybrid perovskites. $MA_{0.5}$ $MA_{0.5}SnI_3$ undergoes a transition from Pm-3m to Im-3 at 0.5 GPa as $MASnI_3$, but it then becomes tetragonal (S.G., $I4/mmm$) at 0.8 GPa and amorphous at 4.0 GPa.[92] The bulk modulus of 11.5 (7) GPa is slightly smaller than the one reported for $MASnI_3$, but pure $FASnI_3$ has a much smaller K_0 of 8.0(7), suggesting that the larger organic cation decreases the stability of the framework.[92] $FASnBr_3$ instead undergoes a phase transition from cubic to orthorhombic at ≈1.8 GPa, coupled with a 0.8 eV redshift of the bandgap, followed by a blueshift.[96] This trend was attributed by DFT to contraction of Sn—Br bond lengths and in particular to the variation in short-long Sn—Br distances.[96] All-inorganic perovskites such as $CsSnBr_3$ show some similarities with their hybrid counterparts. $CsSnBr_3$ is cubic, (S.G. Pm-3m), at ambient conditions and transforms at 0.37 GPa into a tetragonal phase with space group $P4/mbm$.[94] It then undergoes two phase transitions at 1.2 GPa in a monoclinic phase and into a disordered phase at 1.8 GPa.[94] As in the case of $MASnBr_3$, the system shows a good resistance to amorphization.[94] The PL signal of $CsSnBr_3$ diminishes rapidly upon compression and disappears above 1.4 GPa after the tetragonal-to-monoclinic phase transition; a similar effect is present in the absorption spectroscopy data, where the bandgap energy progressively decreases approaching the

Table 1. Pressure-Induced phase transitions.

Composition	Pressure-induced phase transitions	PTM	Methodology	Reference
$MASnI_3$	$Pm\bar{3}m \rightarrow Im\bar{3} \rightarrow Immm$	Fluorinated polymer	Synchrotron XRPD	[92]
$MASnI_3$	$P4mm \rightarrow Pmna$	Silicone oil	Synchrotron XRPD	[84]
$MASnBr_3$	$Pm\bar{3}m \rightarrow$ orthorhombic	Helium	Synchrotron XRPD	[94]
$MASnCl_3$	$Pc \rightarrow P1$	Silicone oil	Synchrotron XRPD	[95]
$MA_{0.5}FA_{0.5}SnI_3$	$Pm\bar{3}m \rightarrow Im\bar{3} \rightarrow I4/mmm$	Fluorinated polymer	Synchrotron XRPD	[92]
$MAGeI_3$	$R3m \rightarrow P4bm$	Neon	Synchrotron XRD	[100]
$FASnI_3$	$Pm\bar{3}m \rightarrow Im\bar{3} \rightarrow I4/mmm$	Fluorinated polymer	Synchrotron XRPD	[92]
$FASnBr_3$	$Pm\bar{3}m \rightarrow Pnma$	Helium	Synchrotron XRPD	[96]
$FAGeI_3$	$R3m$	Neon	Synchrotron XRD	[100]
$CsSnBr_3$	$Pm\bar{3}m \rightarrow P4/mbm \rightarrow$ orthorhombic	Helium	Synchrotron XRPD	[94]
$CsGeBr_3$	$R3m \rightarrow Pm\bar{3}m$	Paraffin	Single crystal XRD	[97]
$CsGeCl_3$	$R3m \rightarrow Pm\bar{3}m$	CsCl and paraffin	Raman/absorption spectroscopy	[98]
$CsGeI_3$	$R3m$	Neon	Synchrotron XRD	[100]
$Cs_2AgBiBr_6$	$Fm\bar{3}m \rightarrow I4/m$	Silicone oil	Synchrotron XRPD	[103]
$Cs_2AgBiCl_6$	$Fm\bar{3}m \rightarrow I4/m$	Silicone oil	Synchrotron XRPD	[104]
Cs_2SnI_6	$Fm\bar{3}m \rightarrow I2/m$	Helium	Synchrotron XRPD	[105]
Cs_2SnCl_6	$Fm\bar{3}m$	Silicone oil	Synchrotron XRPD	[105]
Cs_2SnBr_6	$Fm\bar{3}m$	Silicone oil	Synchrotron XRPD	[105]
$(EDBE)CuCl_4$[a)]	$Pcnn \rightarrow Pnma/Pnna \rightarrow \gamma -$ Phase	None	Synchrotron XRPD	[107]
$(C_4N_2H_14)CuCl_4$	$P2_1/a \rightarrow P2$	Silicone oil	Synchrotron XRPD	[110]
$(C_4N_2H_14)SnBr_4$	$I2/m \rightarrow P\bar{1}$	Silicone oil	Synchrotron XRPD	[111]
$MA_3Bi_2Br_9$	$P\bar{3}m1 \rightarrow P2_1/a$	Silicone oil	Synchrotron XRPD	[113]
$MA_3Bi_2I_9$	$P6_3/mmc \rightarrow P2_1$	Silicone oil	Synchrotron XRPD	[112]
$Cs_3Bi_2Br_9$	$P\bar{3}m1$	Silicone oil	Synchrotron XRPD	[113]
$Cs_3Bi_2I_9$	$P6_3/mmc$	Silicone oil	Synchrotron XRPD	[114]
$Cs_3Sb_2I_9$	$P6_3/mmc$	Silicone oil	Synchrotron XRPD	[115]
$(NH_4)_2SeBr_6$	$Fm\bar{3}m \rightarrow P42$	Silicone oil	Synchrotron XRPD	[116]

[a)] EDBE = 2,2′-(ethylenedioxy)bis(ethylammonium).

transition, as a consequence of the contraction of the Sn—Br bond lengths.[94] $CsGeBr_3$ and $CsGeCl_3$ crystallize in space group $R3m$ and transform to the cubic $Pm\bar{3}m$ structure at 1 and 3 GPa, respectively.[97,98] Upon compression, the rhombohedral angle α increases and the Br–Ge–Br angle decreases till 1 GPa, when the α changes discontinuously to 90°.[97] Absorption spectroscopy shows that the gap of $CsGeBr_3$ decreases with a rate of −0.61 eV/GPa during compression from the ambient conditions value of 2.32(5) eV, whereas the one of $CsGeCl_3$ decreases of about 2.5 eV from ambient pressure to 6 GPa.[98] In the case of $CsGeBr_3$, the possibility of a pressure-driven insulator-to-metal transition was taken into account, but reflectivity measurements up to 30 GPa do not show any evidence of such transition.[98] This possibility was not verified experimentally for $CsGeCl_3$, but a recent theoretical study predicts the semiconducting-metallic transition above 20 GPa.[99] The optical absorption and conductivity are also predicted to increase remarkably in the visible region upon compression, suggesting that performance of a $CsSnCl_3$ perovskite solar cell would be greatly improved by pressure.[99] $AGeI_3$ compounds with A = MA, FA, Cs also crystallize in space group $R3m$ and are characterized by large off-centering of the metal atom.[100] Both $MAGeI_3$ and $FAGeI_3$ show no PL signal at ambient conditions, but this can be turned on upon compression with threshold values higher for $FAGeI_3$ because the larger FA cation induced a large distortion in the octahedra.[100] It is worth noting that PL can be induced by Cs substitution in the system $MA_{1-x}Cs_xGeI_3$ with $x = 0$, 0.2, 0.4, 0.6, 0.8, and 1, the emission intensity increases, while the distortion decreases, with the Cs content, providing an interesting example of combination of chemical and pressure tuning.[100]

2.2. Other Structures

All-inorganic double perovskites structures have also been investigated as possible alternative to lead-based materials. In particular, $Cs_2AgBiBr_6$ and $Cs_2AgBiCl_6$ have shown interesting properties such as long carrier recombination lifetime and good stability, but have large bandgap values.[101,102]

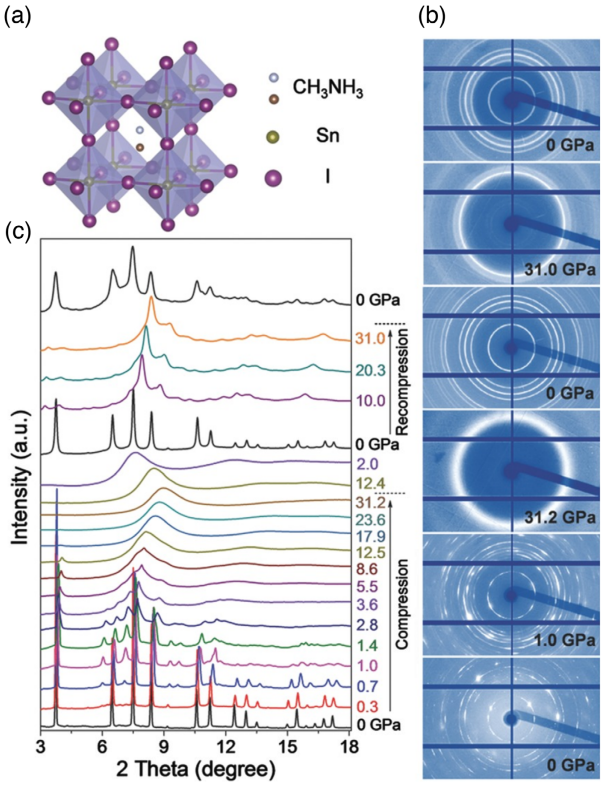

Figure 1. a) Structural sketch of $MASnI_3$. b) 2D synchrotron XRD images at six selected pressures and c) integrated 1D XRD patterns during two sequential compression–decompression cycles. Reproduced with permission.[84] Copyright 2016, Wiley.

$Cs_2AgBiBr_6$ at ambient conditions crystallizes in space group $Fm\bar{3}m$, is orange yellow in color, and has bandgap energy of 2.19 eV.[103] Upon compression up to 2.8 GPa, the absorption edge of $Cs_2AgBiBr_6$ shows little redshift, accompanied by a small narrowing of the bandgap, whereas the crystal color does not change. At 3.2 GPa, the bandgap shows a discontinuity, and then remains unchanged up to 4.0 GPa. Above 4.0 GPa, an abrupt blueshift is detected, and the crystal becomes lighter in color.[103] At 4.5 GPa, $Cs_2AgBiBr_6$ transforms to a tetragonal phase with space group $I4/m$. The phase transition induces octahedral titling in the ab plane, thus shortening the a and b axes. The Bi—Br—Ag bond angle decreases only in the ab plane, whereas the Bi—Br—Ag bond along the c axis remains approximately 180°, thus minimizing octahedral tilting (**Figure 3**).[103] With further compression above 6.5 GPa, the sample exhibits continuous redshift of absorption edge with bandgap narrowing from 2.3 to 1.7 eV at 15 GPa, and the crystal color gradually darkens.[103] The decrease in the bandgap was related to amorphization and the narrowing is partially retained upon pressure release.[103]

$Cs_2AgBiCl_6$ also undergoes a phase transition from a cubic $Fm\bar{3}m$ structure to a tetragonal one with space group $I4/m$ at 5.6 GPa.[104] Amorphization starts around 14 GPa and is complete at 31 GPa. Analogously, the Bi—Cl—Ag bond along the c axis remains 180°, whereas the $BiCl_6$ and $AgCl_6$ octahedra are slightly distorted with different Bi(Ag)—Cl bond lengths in the ab plane with respect to the bonds along the c axis, corresponding to a PL redshift and absorption edge blueshift.[104] In this system, a strong electron–phonon is present, which is enhanced by rotation and distortion of the octahedra, giving redshift and broadening from about 5–7.5 GPa.[104] High pressure can effectively reduce the electron–phonon coupling strength in the cubic phase, whereas it is enhanced in the tetragonal

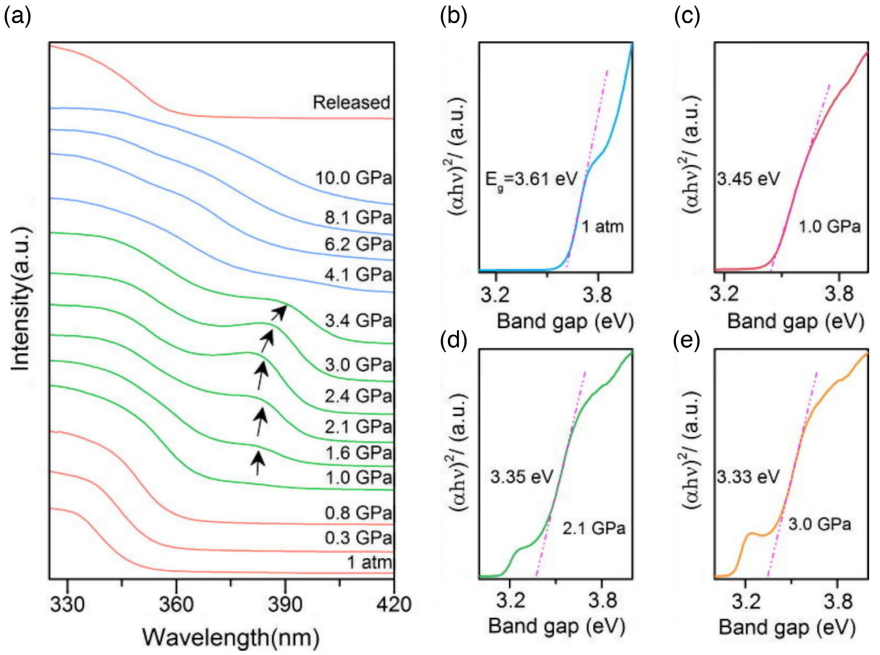

Figure 2. a) Pressure-dependent optical absorption spectroscopy of $MASnCl_3$. b–e) Direct bandgap Tauc plots of $MASnCl_3$ at 1 atm, 1.0, 2.1, and 3.0 GPa. Reproduced with permission.[95] Copyright 2017, AIP Publishing.

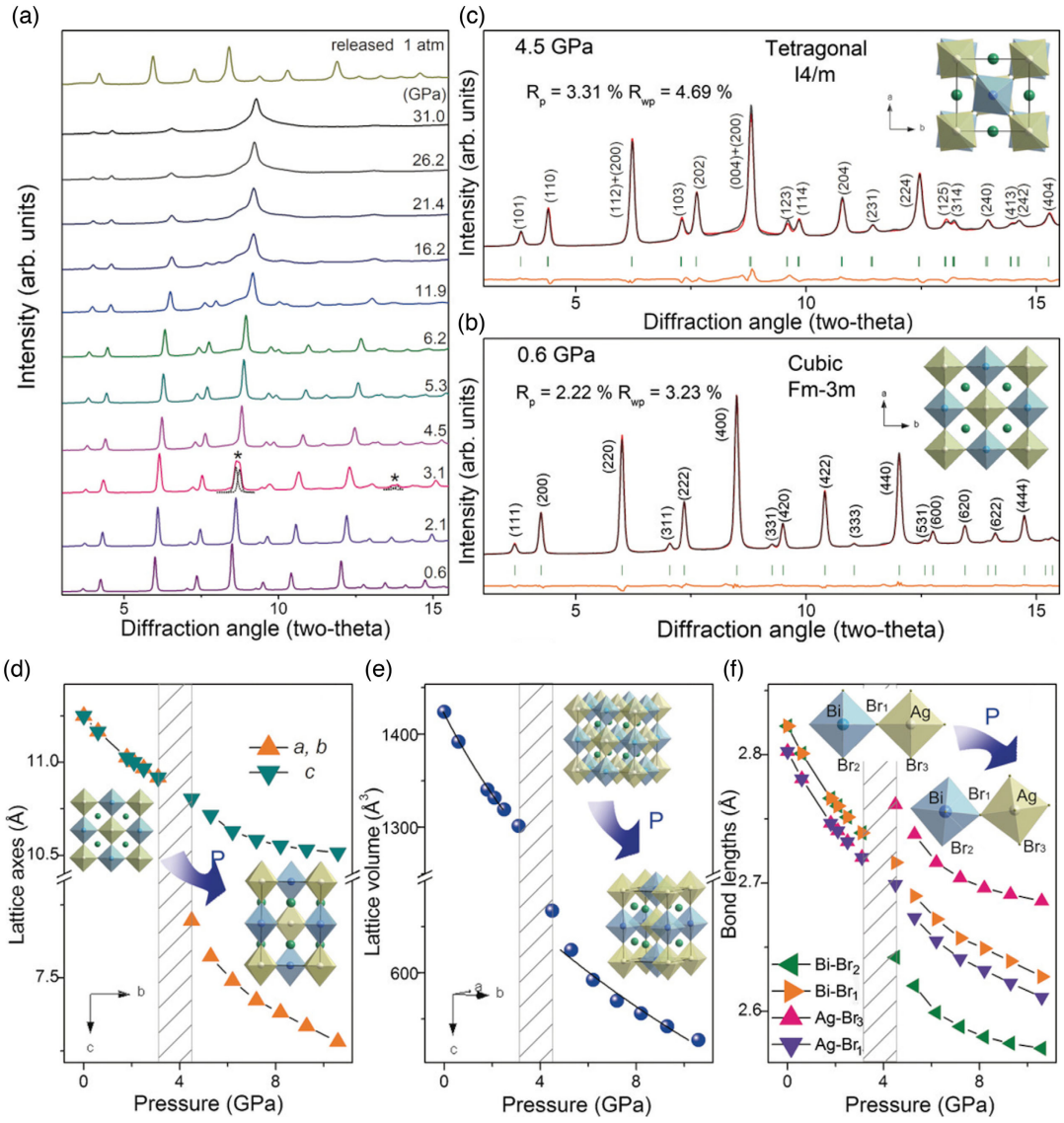

Figure 3. a) Representative patterns of $Cs_2AgBiBr_6$ upon compression. b,c) Rietveld refinements of patterns collected at 0.6 and 4.5 GPa, respectively. The orange lines denote the difference between the observed (black) and the simulated (red) profiles, and the green verticals stand for the simulated peak positions. The purple dotted line represents the amorphous background in profile. The inset shows the corresponding crystal structure. d,e) Evolution of lattice parameters at high pressure. f) Lengths of Bi—Br and Ag—Br bonds as a function of pressure. The shadow marks the phase transition region. Reproduced with permission.[103] Copyright 2017, Wiley.

phase, thus tuning the properties of the material and allowing to directly relate to structure and physical properties.

Vacancy-ordered perovskites are characterized by the B-site cation that is partially replaced with a vacancy. Among this type of metal halide perovskites, the Cs_2BX_6 group, in which half of the B-site cations are occupied by M(IV) cations and the other half by vacancies, has been widely characterized. At high pressure Cs_2BX_6, with X = I, Br, Cl, was studied by a combination of synchrotron XRPD and Raman spectroscopy up to 20 GPa.[105] The three compounds all crystallize in space group $Fm\bar{3}m$, but show a different response to pressure.

Cs_2SnI_6 exhibits some peculiar features in the Raman scattering at 3.3 GPa that suggest the occurrence of a gradual phase transition to a disordered state, marked by the vanishing of the strongest Sn—I symmetric and asymmetric stretching modes and strong reduction of the frequency versus pressure slopes, whereas the diffraction pattern shows a reduction in the compressibility of the crystal.[105] Upon further compression, both Raman spectroscopy and XRD show a transition to a lower symmetry phase in the monoclinic space group $I2/m$, resulting from tilting of the SnI_6 octahedra about the *b* axis. On the contrary, Cs_2SnCl_6 and Cs_2SnBr_6 do not show pressure-induced phase transition up to 12 GPa because of the lower polarizability of chlorine and bromine relative to iodine atoms.[105]

Octahedral titling and metal halide bond contraction have been extensively characterized in perovskites and perovskite derivatives

containing transition metals.[106] Concerning high-pressure studies, there is a lively debate on the possibility to overcome the electronic stabilization from Jahn–Teller (JT) distortion by mechanical compression.[74,107–109] Cu—Cl materials represent an interesting case because they have a half-filled band that could provide a conduction pathway, where JT distortion reduces the orbital overlap, contributing to the insulating behavior. $(EDBE)CuCl_4$ was studied up to 60 GPa and shows reversible color changes from translucent yellow to red to opaque black.[107] Compression of the yellow phase induces a transition to a translucent red sample at ≈4 GPa, then upon further compression two successive transformation are detected at 7 and 9 GPa.[107] Above this pressure, the resulting phase is much less compressible and shows sufficient orbital overlap for charge carrier mobility, and the color changes to opaque black, together with a loss of signal in the Raman spectrum.[107] At high pressure, the electrical conductivity is at least five orders of magnitude higher, up to 2.9×10^{-4} S cm^{-1} at 51.4 GPa, and the bandgap is 1.0 eV at 39.7 GPa, suggesting that high pressure can improve the *d*-orbital overlap by compressing the structure, through octahedral tilting and Cu—Cl bond shortening.[107] Another system of interest for photovoltaic applications, where the effect of pressure on JT distortion was characterized, is $(C_4N_2H_14)CuCl_4$.[110] At high pressure, the bandgap narrows from 2.45 to 2.05 eV as a result of the shrinkage and distortion of the inorganic framework, including a phase transition between 6.4 and 10.5 GPa.[110] This material also shows a relatively high resistance to amorphization because it maintains its structural integrity at least up to 12 GPa due to the long organic chains that act as spring cushion, suggesting that the length of organic chains could play a major role in the structure and bandgap behaviors at high pressure.[110] The same organic cation was also used in a tin-based perovskite derivative $(C_4N_2H_14)SnBr_4$ studied at high pressure.[111] Upon compression, the sample does not show a variation in the PL up to 2.06 GPa, when a broadband emission appears, and then exhibits a persistent increase with increasing pressure, until it reaches the maximum at about 8.01 GPa.[111] Interestingly, the absorption edge shows a gradual redshift together with a bandgap narrowing of approximately 0.25 eV until 2.07 GPa. Upon further pressure increase, the profile of the absorption edge exhibits a tiny blueshift, in good agreement with the appearance of broadband emission.[111] When the pressure reaches 3.52 GPa, the absorption edge continuously redshifts again up to 19.02 GPa. The changes in the optical properties can be related to variation in the diffraction patterns because peak splitting at 1.99 GPa marks the beginning of a phase transition from the monoclinic $I2/m$ phase to the triclinic $P\bar{1}$ phase that is completed at 3.50 GPa.[111] Above 14.80 GPa, amorphization starts, but the absorption spectrum is restored back to the initial state upon pressure release.[111] Bi and Sb have also been considered as alternative to Pb for photovoltaic materials. $MA_3Bi_2I_9$ was characterized by means of different techniques in a large pressure range.[112] At ambient conditions, the sample shows a broad emission and weak PL intensity, but upon compression the PL experiences a gradual redshift and a large enhancement, reaching a peak value at 2.5 GPa and then weakening until complete disappearance at 9.0 GPa.[112] Interestingly, the absorption edge gradually redshifts, then moving into the near-infrared above 9.6 GPa, to finally shift into the near-infrared at 16.9 GPa.[112] When the pressure is released, the absorption spectrum goes back to its initial state, suggesting a reversible process.[112] The bandgap varies from 2.09 eV at ambient pressure and narrows at rate of 23.5 meV GPa^{-1} below 5 GPa and of 76.3 meV GPa^{-1} at higher pressure indicating a possible change in the electronic structure.[112] At 13.2 GPa the bandgap reaches a value of 1.35 eV. The variation in the bandgap can be related with piezochromism with the sample changing color from transparent red at ambient pressure to opaque black at 11 GPa.[112] At ambient conditions, $MA_3Bi_2I_9$ crystallizes in a $P6_3/mmc$ phase, characterized by face-sharing Bi_2I_9 clusters separated by MA cations, thus assuming a structure clearly different from the 3D perovskite structure, with slightly distorted BiI_6 octahedra with three longer equivalent bridging Bi—I bonds and three shorter equivalent terminal Bi—I bonds along the *c* direction.[112] At 5 GPa $MA_3Bi_2I_9$ transforms into the $P2_1$ phase, and the BiI_6 octahedron becomes more distorted because the organic cations are ordered and gain a preferential orientation along the *b* axis.[112] As a consequence, the Bi_2I_9 units can be considered as a periodic arrangement of quantum dots (QDs) surrounded by insulating organic groups below 15 GPa, but upon further pressure increase the amorphous phase begins to emerge, starting to break the long-range order of the "QDs," till complete amorphization at 29 GPa (**Figure 4**).[112] When the pressure is released, the sample reverts to its initial state.[112] Measurements of the electrical resistance as a function of pressure show poor electronic transport ability at low pressure, as a consequence of isolated Bi—I inorganic framework. Increasing the pressure, the resistance decreases and reaches a minimum of 19 Ω at 65 GPa.[112] Temperature-dependent resistance measurement during compression shows that the sample is still semiconducting at 56 GPa, but starting from

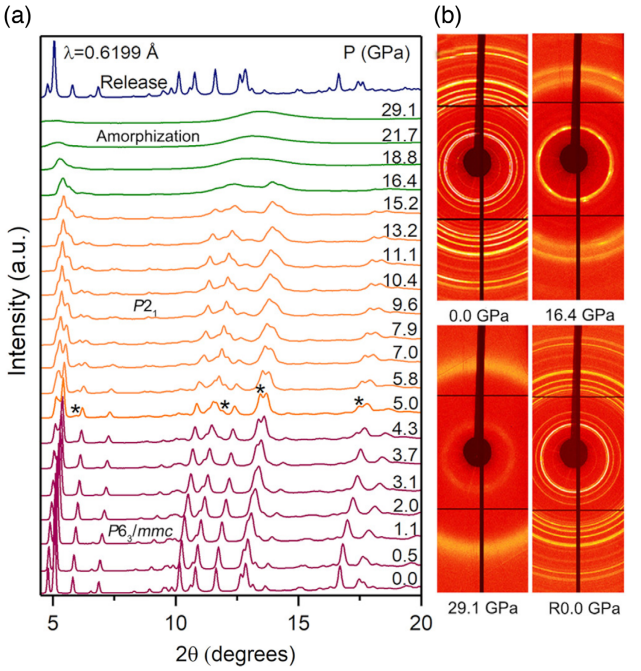

Figure 4. a) Synchrotron XRD patterns of $MA_3Bi_2I_9$ as a function of pressure. b) Selected 2D XRD images at varying pressures. "R" marks pattern collected on pressure release. Reproduced with permission.[112] Copyright 2019, American Chemical Society.

60 GPa the resistance increases upon heating suggesting a metallic character.[112]

Replacing Br with I gives a different structure because $MA_3Bi_2Br_9$ crystallizes in a trigonal phase $P\bar{3}m1$ with layers of corner-shared $BiBr_6$ octahedra connected by Bi—Br—Bi bond angles of 180°. Between 4.3 and 5.0 GPa, the sample transforms to a monoclinic structure with space group $P2_1/a$, with increased distortion and tilting of the octahedra.[113] At ambient conditions, $MA_3Bi_2Br_9$ is light yellow and has a bandgap of 2.65 eV that narrows of 0.2 eV up to 4.1 GPa, due to overlap of Bi and Br orbitals promoted by the contraction of the octahedra and of the Bi—Br—Bi bonds.[113] In the transition range between 4.6 and 5.5 GPa, a blueshift is observed at the absorption edge and the bandgap slightly widens, as a result of the larger octahedral tilting that decreases the coupling between Bi and Br orbitals.[113] The main contribution of the organic cation is to provide flexibility to the structure, as clearly emerges replacing the MA cation with Cs.[113] $Cs_3Bi_2Br_9$ crystallizes in the same space group as $MA_3Bi_2Br_9$, but has a larger bulk modulus, more rigid axial contraction, and smaller axial compressibility, due to the stronger covalent interactions between Cs^+ and $BiBr_6$.[113] This trend is confirmed by $Cs_3Bi_2I_9$[114,115] $Cs_3Sb_2I_9$ with bulk moduli of 23.7 and 24.7 GPa, respectively. $Cs_3Bi_2I_9$ shows a weak red PL that has a sharp increase under mild pressure, followed by a gradual decrease until it completely disappears at 9.3 GPa.[114] The emission spectra maintain a continuous slow redshift during compression from the visible region to the near-infrared region.[114] At 13 GPa, the absorption edge shows a very sharp redshift, suggesting the occurrence of a transition, and the absorption spectrum returns to the initial state upon decompression.[114] At ambient conditions $Cs_3Bi_2I_9$ has a bandgap of 2.06 eV that decreases to 1.12 eV at 12.1 GPa,[114] while the resistance is high and increases slightly until a peak value is reached at about 7.0 GPa, and then decreases continuously and rapidly, reaching a minimum value of 33 Ω at 28 GPa. At this pressure, the electrical resistance increases with increasing temperature, suggesting a semiconductor-to-metal transition.[114] $Cs_3Sb_2I_9$ exhibits a similar behavior with the bandgap that narrows from 2.34 to 1.68 eV from ambient conditions to 14 GPa. It is worth noting that $Cs_3Sb_2I_9$ shows a larger bandgap change than $MA_3Bi_2Br_9$ because the large MA cation makes the structure more compressible.[115] Analogously, Sb^{3+} cations have smaller ionic radius than Bi^{3+} that results in better structural stability at higher pressure and a larger bandgap change for $Cs_3Sb_2I_9$.[115] Selenium has also been considered as an alternative to lead, in particular in the vacancy ordered $(NH_4)_2SeBr_6$ perovskite.[116] At room conditions the compound is cubic with space group $Fm\bar{3}m$, and transforms to a tetragonal $P42$ phase above 11 GPa as a result of the rotation of the $[SeBr_6]^{2-}$ octahedra.[116] The cubic and the tetragonal phases have bulk moduli of 22.28 and 131.91 GPa, respectively, suggesting that the tetragonal phase has a more robust structure that could contribute to the stability of the solar cell.[116]

3. From Fundamental Studies to Applications

Despite the promising and interesting results obtained in situ, there is still a gap between fundamental studies and actual applications in operating devices. One of the main reasons is the difficulty to retain the desired properties obtained at high pressure back to ambient conditions. In this respect, different strategies have been developed. $CsPbI_3$ is a good example because it has four polymorphs with the δ-phase easily accessible room conditions that does not crystallize in the perovskite structure, whereas the high-temperature phases, α, β, and γ, are perovskites and show more desirable optical and conductivity properties. Different solutions have been tested to try and stabilize these materials, such as thermal treatments[117] or strain-engineering.[118] The proposed protocols for thermal engineering are based on solid-state methods that require rigorously anhydrous reagents and a moisture-free environment, but the obtained samples of $\gamma - CsPbI_3$ are very sensitive to moisture.[117] Alternatively, a strain can be induced in a thin film of $CsPbI_3$ through annealing and rapidly cooling, but the product also presents stability issues and quickly transforms to the δ-phase in presence of humidity.[118] A different route to the stabilization of the desired phase might be high pressure, as proposed by recent works.[91] The authors applied a pressure between 0.1 and 0.6 GPa to δ-phase-$CsPbI_3$ followed by heating and rapid quenching. The resulting $\gamma - CsPbI_3$ can be retained after releasing pressure to ambient conditions and, in contrast with the previous methods, it shows a good stability to air moisture for up to 10 days.[91] These approaches are still poorly tested on lead-free perovskites and are mostly limited to cycles of compression and decompression, as performed on $MASnI_3$[84,119] $(BA)_2(MA)_2Pb_3I_10$. In the second case, the pressure treatment was applied to the compounds series $(BA)_2(MA)_{n-1}Pb_nI_{3n+1}$ with n = 1, 2, 3, 4 and a long-term large bandgap narrowing, from 1.94 to 1.78 eV, was obtained for the $n = 3$ composition after compression to 26 GPa followed by decompression down to ambient pressure.[119] The bandgap narrowing was attributed to the widening of Pb—I—Pb bond angles and a large overlap between the Pb and I orbitals.[119] The authors also reported that this pressure treatment is effective in 2D perovskites with an optimal n value, where 3 represents a threshold above which lower phase transition or atomic distortion during compression can hinder the retention of the desired properties.[119] Pressure can be also applied ex situ, as in the case of $MAPbI_3$.[120] The samples can be compressed for 5 min and then the pressure is quickly released (**Figure 5**) in a sort of "pressure quenching" approach.[120] This treatment allows to retain lattice shrinkage and modulation of the bandgap that are stable at least for 15 days.[120]

Some few works also tried to exploit the use of pressure directly on PSCs.[121] By applying a pressure from 0 to 7 MPa to a device based on MAPbI3, an improvement of the photoconversion efficiencies up to 40% was observed. Such an effect was related to both an improved interlayer surface contacts and an improvement of the optical properties by a reduction of the bandgap, as observed by DAC experiments.[121] The effect of pressing, as part of the common encapsulation process of perovskite solar cells, was investigated.[122] Pressures equal to 400–500 mbar were reported to have a positive effect on the efficiency mainly from reduced series resistance.[122] The improvement is mostly related to improved interfaces rather than the perovskite layer itself, suggesting that a properly designed encapsulation process could be beneficial to a wide range of different perovskite materials regardless of their composition.[122]

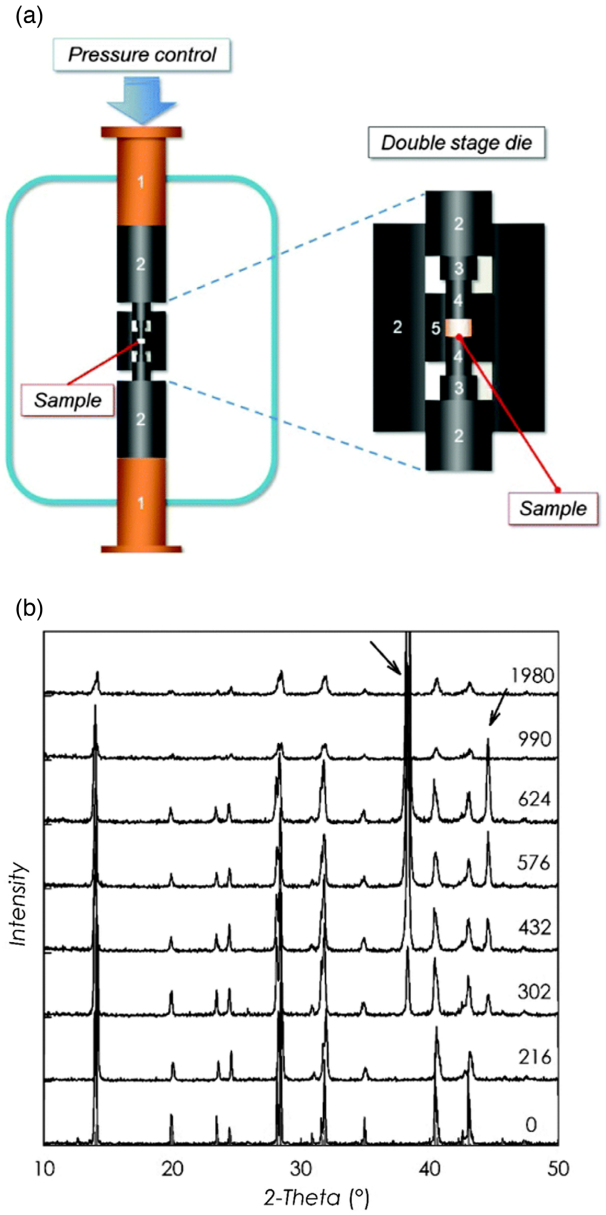

Figure 5. a) Scheme of the high pressure apparatus. The external rams applying the uniaxial pressure are made of copper (1). The double stage die is mainly made of graphite (2), with the exception of the inner parts (3, 4, and 5) which are made of SiC or WC; b) XRD patterns of $MAPbI_3$ samples with the corresponding compression pressures in MPa. Vertical red bars: reference patterns for tetragonal MAPI. Arrows in the figure refer to sample-holder signals. Reproduced with permission.[120] Copyright 2018, The Royal Society of Chemistry.

4. Conclusion and Outlook

This review shows how high pressure can be used to explore the stability, phase diagram, and structure–properties relationship in lead-free metal halides and to tune their physical properties. Despite such studies can provide useful information and unveil exciting novel properties, this approach is still poorly explored in lead-free perovskites with respect to their lead-containing counterparts. Being able to understand the pressure-induced changes allows, for example, to exploit chemical pressure, that is, using atoms or molecules of mismatched size to induce a strain in the structure. As it is known that chemical pressure tends to mimic the effects of mechanical pressure,[123,124] high pressure studies can be used to systematically explore structure–properties relationship and once a desired property is identified this could be reproduced by chemical pressure. It also worth noting that high-pressure treatments, being a physical process, are inherently environmentally friendly because they do not require the use of potentially harmful solvents or purification to remove byproducts. One of the main drawbacks in practical applications of the results of high-pressure studies is the limited size of the sample, typical of DACs. Because of the design of DACs, the sample is generally very small, of the order of tens of micrometers. The use of larger apparatus that still allows to apply large pressure, such as a large-volume press, is desirable in this respect because it easily opens to the possibility of obtaining larger samples, above the millimeters scale size. Another possible approach is to apply pressure ex situ to access high-pressure properties at room conditions for example by strain engineering. It is clear that opening the way to take advantage of the superior and appealing properties shown by lead-free MHPs at high pressure could provide a revolution in the development of efficient photovoltaic devices. It would be highly desirable to see, in the forthcoming years, more applied research aiming at devising strategies to stabilize the high-pressure phenomena at ambient conditions.

Acknowledgements

Open Access Funding provided by Universita degli Studi di Pavia within the CRUI-CARE Agreement.

Conflict of Interest

The authors declare no conflict of interest.

Keywords

high pressure, hybrid perovskites, lead free perovskites

Received: July 18, 2021
Revised: September 21, 2021
Published online: October 4, 2021

[1] A. Kojima, K. Teshima, Y. Shirai, T. Miyasaka, *J. Am. Chem. Soc.* **2009**, *131*, 6050.
[2] C. C. Stoumpos, M. G. Kanatzidis, *Acc. Chem. Res.* **2015**, *48*, 2791.
[3] H. Lin, C. Zhou, Y. Tian, T. Siegrist, B. Ma, *ACS Energy Lett.* **2018**, *3*, 54.
[4] G. Grancini, M. K. Nazeeruddin, *Nat. Rev. Mater.* **2019**, *4*, 4.
[5] Y.-T. Huang, S. R. Kavanagh, D. O. Scanlon, A. Walsh, R. L. Z. Hoye, *Nanotechnology* **2021**, *32*, 132004.
[6] J. Breternitz, S. Schorr, *Adv. Energy Mater.* **2018**, *8*, 1802366.
[7] Q. A. Akkerman, L. Manna, *ACS Energy Lett.* **2020**, *5*, 604.
[8] V. M. Goldschmidt, *Naturwissenschaften* **1926**, *14*, 477.
[9] A. M. Glazer, *Acta Crystallogr. Sect. B Struct. Crystallogr. Cryst. Chem.* **1972**, *28*, 3384.

[10] G. Volonakis, M. R. Filip, A. A. Haghighirad, N. Sakai, B. Wenger, H. J. Snaith, F. Giustino, *J. Phys. Chem. Lett.* **2016**, *7*, 1254.
[11] D. B. Mitzi, *J. Chem. Soc. Dalton Trans.* **2001**, *1*, 1.
[12] D. B. Mitzi, C. D. Dimitrakopoulos, L. L. Kosbar, *Chem. Mater.* **2001**, *13*, 3728.
[13] J. L. Knutson, J. D. Martin, D. B. Mitzi, *Inorg. Chem.* **2005**, *44*, 4699.
[14] K.-z. Du, Q. Tu, X. Zhang, Q. Han, J. Liu, S. Zauscher, D. B. Mitzi, *Inorg. Chem.* **2017**, *56*, 9291.
[15] P.-X. Wang, A. M. Najarian, Z. Hao, A. Johnston, O. Voznyy, S. Hoogland, E. H. Sargent, *J. Phys. Chem. Lett.* **2020**, *11*, 10144.
[16] D. Cortecchia, S. Neutzner, A. R. Srimath Kandada, E. Mosconi, D. Meggiolaro, F. De Angelis, C. Soci, A. Petrozza, *J. Am. Chem. Soc.* **2017**, *139*, 39.
[17] W. Shockley, H. J. Queisser, *J. Appl. Phys.* **1961**, *32*, 510.
[18] S. Rühle, *Solar Energy* **2016**, *130*, 139.
[19] J. Jeong, M. Kim, J. Seo, H. Lu, P. Ahlawat, A. Mishra, Y. Yang, M. A. Hope, F. T. Eickemeyer, M. Kim, Y. J. Yoon, I. W. Choi, B. P. Darwich, S. J. Choi, Y. Jo, J. H. Lee, B. Walker, S. M. Zakeeruddin, L. Emsley, U. Rothlisberger, A. Hagfeldt, D. S. Kim, M. Grätzel, J. Y. Kim, *Nature* **2021**, *592*, 7854.
[20] M. Grätzel, *Nat. Mater.* **2014**, *13*, 838.
[21] A. Babayigit, A. Ethirajan, M. Muller, B. Conings, *Nat. Mater.* **2016**, *15*, 247.
[22] Y. Jiang, L. Qiu, E. J. Juarez-Perez, L. K. Ono, Z. Hu, Z. Liu, Z. Wu, L. Meng, Q. Wang, Y. Qi, *Nat. Energy* **2019**, *4*, 585.
[23] X. Li, F. Zhang, H. He, J. J. Berry, K. Zhu, T. Xu, *Nature* **2020**, *578*, 555.
[24] J. Li, J. Duan, X. Yang, Y. Duan, P. Yang, Q. Tang, *Nano Energy* **2021**, *80*, 105526.
[25] T. Umebayashi, K. Asai, T. Kondo, A. Nakao, *Phys. Rev. B* **2003**, *67*, 155405.
[26] F. Hao, C. C. Stoumpos, D. H. Cao, R. P. H. Chang, M. G. Kanatzidis, *Nat. Photonics* **2014**, *8*, 489.
[27] W. Ke, C. C. Stoumpos, M. G. Kanatzidis, *Adv. Mater.* **2019**, *31*, 1803230.
[28] M. Wang, W. Wang, B. Ma, W. Shen, L. Liu, K. Cao, S. Chen, W. Huang, *Nano-Micro Lett.* **2021**, *13*, 62.
[29] T. Miyasaka, A. Kulkarni, G. M. Kim, S. Öz, A. K. Jena, *Adv. Energy Mater.* **2020**, *10*, 1902500.
[30] H. Fu, *Solar Energy Mater. Solar Cells* **2019**, *193*, 107.
[31] F. Sani, S. Shafie, H. N. Lim, A. O. Musa, *Materials* **2018**, *11*, 1008.
[32] S. F. Hoefler, G. Trimmel, T. Rath, *Monatshefte Chem. Chem. Monthly* **2017**, *148*, 795.
[33] D. Sabba, H. K. Mulmudi, R. R. Prabhakar, T. Krishnamoorthy, T. Baikie, P. P. Boix, S. Mhaisalkar, N. Mathews, *J. Phys. Chem. C* **2015**, *119*, 1763.
[34] Y. Zhao, K. Zhu, *Chem. Soc. Rev.* **2016**, *45*, 655.
[35] Z. Zhao, F. Gu, Y. Li, W. Sun, S. Ye, H. Rao, Z. Liu, Z. Bian, C. Huang, *Adv. Sci.* **2017**, *4*, 1700204.
[36] I. C. Smith, E. T. Hoke, D. Solis-Ibarra, M. D. McGehee, H. I. Karunadasa, *Angew. Chem., Int. Ed.* **2014**, *126*, 11414.
[37] F. Wang, X. Jiang, H. Chen, Y. Shang, H. Liu, J. Wei, W. Zhou, H. He, W. Liu, Z. Ning, *Joule* **2018**, *2*, 2732.
[38] D. B. Mitzi, *Chem. Mater.* **1996**, *8*, 791.
[39] Y. Gao, Z. Wei, P. Yoo, E. Shi, M. Zeller, C. Zhu, P. Liao, L. Dou, *J. Am. Chem. Soc.* **2019**, *141*, 15577.
[40] A. Pisanu, M. Coduri, M. Morana, Y. O. Ciftci, A. Rizzo, A. Listorti, M. Gaboardi, L. Bindi, V. I. E. Queloz, C. Milanese, G. Grancini, L. Malavasi, *J. Mater. Chem. A* **2020**, *8*, 1875.
[41] Y. Liao, H. Liu, W. Zhou, D. Yang, Y. Shang, Z. Shi, B. Li, X. Jiang, L. Zhang, L. N. Quan, R. Quintero-Bermudez, B. R. Sutherland, Q. Mi, E. H. Sargent, Z. Ning, *J. Am. Chem. Soc.* **2017**, *139*, 6693.
[42] S. Shao, J. Liu, G. Portale, H.-H. Fang, G. R. Blake, G. H. ten Brink, L. J. A. Koster, M. A. Loi, *Adv. Energy Mater.* **2018**, *8*, 1702019.
[43] X. Jiang, F. Wang, Q. Wei, H. Li, Y. Shang, W. Zhou, C. Wang, P. Cheng, Q. Chen, L. Chen, Z. Ning, *Nat. Commun.* **2020**, *11*, 1.
[44] S. J. Lee, S. S. Shin, Y. C. Kim, D. Kim, T. K. Ahn, J. H. Noh, J. Seo, S. I. Seok, *J. Am. Chem. Soc.* **2016**, *138*, 3974.
[45] R. Chiara, M. Morana, L. Malavasi, *ChemPlusChem* **2021**, *86*, 879.
[46] C. C. Stoumpos, L. Frazer, D. J. Clark, Y. S. Kim, S. H. Rhim, A. J. Freeman, J. B. Ketterson, J. I. Jang, M. G. Kanatzidis, *J. Am. Chem. Soc.* **2015**, *137*, 6804.
[47] S. Yue, S. C. McGuire, H. Yan, Y. S. Chu, M. Cotlet, X. Tong, S. S. Wong, *ACS omega* **2019**, *4*, 18219.
[48] S. Nagane, D. Ghosh, R. L. Hoye, B. Zhao, S. Ahmad, A. B. Walker, M. S. Islam, S. Ogale, A. Sadhanala, *J. Phys. Chem. C* **2018**, *122*, 5940.
[49] M. Chen, M.-G. Ju, H. F. Garces, A. D. Carl, L. K. Ono, Z. Hawash, Y. Zhang, T. Shen, Y. Qi, R. L. Grimm, D. Pacifici, X. C. Zeng, Y. Zhou, N. P. Padture, *Nat. Commun.* **2019**, *10*, 1.
[50] N. Ito, M. A. Kamarudin, D. Hirotani, Y. Zhang, Q. Shen, Y. Ogomi, S. Iikubo, T. Minemoto, K. Yoshino, S. Hayase, *J. Phys. Chem. Lett.* **2018**, *9*, 1682.
[51] X. Chang, D. Marongiu, V. Sarritzu, N. Sestu, Q. Wang, S. Lai, A. Mattoni, A. Filippetti, F. Congiu, A. G. Lehmann, F. Quochi, M. Saba, A. Mura, G. Bongiovanni, *Adv. Funct. Mater.* **2019**, *29*, 1903528.
[52] P. Cheng, T. Wu, J. Zhang, Y. Li, J. Liu, L. Jiang, X. Mao, R.-F. Lu, W.-Q. Deng, K. Han, *J. Phys. Chem. Lett.* **2017**, *8*, 4402.
[53] P. Cheng, T. Wu, J. Liu, W.-Q. Deng, K. Han, *J. Phys. Chem. Lett.* **2018**, *9*, 2518.
[54] R. Chiara, M. Morana, M. Boiocchi, M. Coduri, M. Striccoli, F. Fracassi, A. Listorti, A. Mahata, P. Quadrelli, M. Gaboardi, C. Milanese, L. Bindi, F. D. Angelis, L. Malavasi, *J. Mater. Chem. C* **2021**, *9*, 9899.
[55] E. T. McClure, M. R. Ball, W. Windl, P. M. Woodward, *Chem. Mater.* **2016**, *28*, 1348.
[56] K.-z. Du, W. Meng, X. Wang, Y. Yan, D. B. Mitzi, *Angew. Chem., Int. Ed.* **2017**, *56*, 8158.
[57] J. Zhou, Z. Xia, M. S. Molokeev, X. Zhang, D. Peng, Q. Liu, *J. Mater. Chem. A* **2017**, *5*, 15031.
[58] C. Chen, T.-H. Han, S. Tan, J. Xue, Y. Zhao, Y. Liu, H. Wang, W. Hu, C. Bao, M. Mazzeo, R. Wang, Y. Duan, Y. Yang, *Nano Lett.* **2020**, *20*, 4673.
[59] X. Yang, Y. Chen, P. Liu, H. Xiang, W. Wang, R. Ran, W. Zhou, Z. Shao, *Adv. Funct. Mater.* **2020**, *30*, 2001557.
[60] K. Eckhardt, V. Bon, J. Getzschmann, J. Grothe, F. M. Wisser, S. Kaskel, *Chem. Commun.* **2016**, *52*, 3058.
[61] B.-W. Park, B. Philippe, X. Zhang, H. Rensmo, G. Boschloo, E. M. Johansson, *Adv. Mater.* **2015**, *27*, 6806.
[62] J.-C. Hebig, I. Kuhn, J. Flohre, T. Kirchartz, *ACS Energy Lett.* **2016**, *1*, 309.
[63] S. M. Jain, D. Phuyal, M. L. Davies, M. Li, B. Philippe, C. De Castro, Z. Qiu, J. Kim, T. Watson, W. C. Tsoi, O. Karis, H. Rensmo, G. Boschloo, T. Edvinsson, J. R. Durrant, *Nano Energy* **2018**, *49*, 614.
[64] W. A. Bassett, *High Pressure Res.* **2009**, *29*, 163.
[65] A. Katrusiak, *Acta Crystallogr. Sect. A Found. Crystallogr.* **2008**, *64*, 135.
[66] H. K. Mao, J. Xu, P. M. Bell, *J. Geophys. Res.* **1986**, *91*, 4673.
[67] S. D. Jacobsen, C. M. Holl, K. A. Adams, R. A. Fischer, E. S. Martin, C. R. Bina, J.-F. Lin, V. B. Prakapenka, A. Kubo, P. Dera, *Am. Min.* **2008**, *93*, 1823.
[68] R. J. Angel, D. R. Allan, R. Miletich, L. W. Finger, *J. Appl. Crystallogr.* **1997**, *30*, 461.
[69] K. S. Scheidl, A. Kurnosov, D. M. Trots, T. Boffa Ballaran, R. J. Angel, R. Miletich, *J. Appl. Crystallogr.* **2016**, *49*, 2129.
[70] P. M. Bell, J.-A. Xu, H. K. Mao, in *Shock Waves in Condensed Matter* (Ed.: Y. M. Gupta), Springer US, Boston, MA **1986**, pp. 125–130.
[71] R. J. Angel, M. Bujak, J. Zhao, G. D. Gatta, S. D. Jacobsen, *J. Appl. Crystallogr.* **2007**, *40*, 26.

[72] S. Klotz, J.-C. Chervin, P. Munsch, G. Le Marchand, *J. Phys. D: Appl. Phys.* **2009**, *42*, 075413.
[73] A. Jaffe, Y. Lin, C. M. Beavers, J. Voss, W. L. Mao, H. I. Karunadasa, *ACS Central Sci.* **2016**, *2*, 201.
[74] A. Jaffe, Y. Lin, H. I. Karunadasa, *ACS Energy Lett.* **2017**, *2*, 1549.
[75] P. Postorino, L. Malavasi, *J. Phys. Chem. Lett.* **2017**, *8*, 2613.
[76] M. Szafrański, A. Katrusiak, *J. Phys. Chem. Lett.* **2017**, *8*, 2496.
[77] X. Lü, W. Yang, Q. Jia, H. Xu, *Chem. Sci.* **2017**, *8*, 6764.
[78] L.-J. Ji, S.-J. Sun, Y. Qin, K. Li, W. Li, *Coord. Chem. Rev.* **2019**, *391*, 15.
[79] M. Li, T. Liu, Y. Wang, W. Yang, X. Lü, *Matter Radiat. Extremes* **2020**, *HPS2020*, 018201.
[80] Y. Shi, Y. Zhou, Z. Ma, G. Xiao, K. Wang, B. Zou, *J. Mater. Chem. C* **2020**, *8*, 12755.
[81] L. Zhang, K. Wang, Y. Lin, B. Zou, *J. Phys. Chem. Lett.* **2020**, *11*, 4693.
[82] G. Liu, L. Kong, J. Gong, W. Yang, H.-k. Mao, Q. Hu, Z. Liu, R. D. Schaller, D. Zhang, T. Xu, *Adv. Funct. Mater.* **2017**, *27*, 1604208.
[83] S. Sun, F. H. Isikgor, Z. Deng, F. Wei, G. Kieslich, P. D. Bristowe, J. Ouyang, A. K. Cheetham, *ChemSusChem* **2017**, *10*, 3740.
[84] X. Lü, Y. Wang, C. C. Stoumpos, Q. Hu, X. Guo, H. Chen, L. Yang, J. S. Smith, W. Yang, Y. Zhao, H. Xu, M. G. Kanatzidis, Q. Jia, *Adv. Mater.* **2016**, *28*, 8663.
[85] S. Liu, S. Sun, C. K. Gan, A. G. d. Águila, Y. Fang, J. Xing, T. T. H. Do, T. J. White, H. Li, W. Huang, Q. Xiong, *Sci. Adv.* **2019**, *5*, 9445.
[86] L. Zhang, Q. Zeng, K. Wang, *J. Phys. Chem. Lett.* **2017**, *8*, 3752.
[87] Y. Ying, X. Luo, H. Huang, *J. Phys. Chem. C* **2018**, *122*, 17718.
[88] G. Yuan, S. Qin, X. Wu, H. Ding, A. Lu, *Phase Trans.* **2018**, *91*, 38.
[89] L. Zhang, L. Wang, K. Wang, B. Zou, *J. Phys. Chem. C* **2018**, *122*, 15220.
[90] J.-H. Lee, N. C. Bristowe, J. H. Lee, S.-H. Lee, P. D. Bristowe, A. K. Cheetham, H. M. Jang, *Chem. Mater.* **2016**, *28*, 4259.
[91] F. Ke, C. Wang, C. Jia, N. R. Wolf, J. Yan, S. Niu, T. P. Devereaux, H. I. Karunadasa, W. L. Mao, Y. Lin, *Nat. Commun.* **2021**, *12*, 461.
[92] Y. Lee, D. B. Mitzi, P. W. Barnes, T. Vogt, *Phys. Rev. B* **2003**, *68*, 020103.
[93] C. C. Stoumpos, C. D. Malliakas, M. G. Kanatzidis, *Inorg. Chem.* **2013**, *52*, 9019.
[94] M. Coduri, T. A. Strobel, M. Szafrański, A. Katrusiak, A. Mahata, F. Cova, S. Bonomi, E. Mosconi, F. De Angelis, L. Malavasi, *J. Phys. Chem. Lett.* **2019**, *10*, 7398.
[95] L. Wang, T. Ou, K. Wang, G. Xiao, C. Gao, B. Zou, *Appl. Phys. Lett.* **2017**, *111*, 233901.
[96] M. Coduri, T. B. Shiell, T. A. Strobel, A. Mahata, F. Cova, E. Mosconi, F. D. Angelis, L. Malavasi, *Mater. Adv.* **2020**, *1*, 2840.
[97] U. Schwarz, H. Hillebrecht, M. Kaupp, K. Syassen, H. G. von Schnering, G. Thiele, *J. Solid State Chem.* **1995**, *118*, 20.
[98] U. Schwarz, F. Wagner, K. Syassen, H. Hillebrecht, *Phys. Rev. B* **1996**, *53*, 12545.
[99] J. Islam, A. K. M. A. Hossain, *Sci. Rep.* **2020**, *10*, 14391.
[100] X. Lü, C. Stoumpos, Q. Hu, X. Ma, D. Zhang, S. Guo, J. Hoffman, K. Bu, X. Guo, Y. Wang, C. Ji, H. Chen, H. Xu, Q. Jia, W. Yang, M. G. Kanatzidis, H.-K. Mao, *Natl. Sci. Rev.* **2020**, nwaa288.
[101] M. R. Filip, S. Hillman, A. A. Haghighirad, H. J. Snaith, F. Giustino, *J. Phys. Chem. Lett.* **2016**, *7*, 2579.
[102] W. Pan, H. Wu, J. Luo, Z. Deng, C. Ge, C. Chen, X. Jiang, W.-J. Yin, G. Niu, L. Zhu, L. Yin, Y. Zhou, Q. Xie, X. Ke, M. Sui, J. Tang, *Nat. Photonics* **2017**, *11*, 726.
[103] Q. Li, Y. Wang, W. Pan, W. Yang, B. Zou, J. Tang, Z. Quan, *Angew. Chem., Int. Ed.* **2017**, *129*, 16185.
[104] L. Zhang, Y. Fang, L. Sui, J. Yan, K. Wang, K. Yuan, W. L. Mao, B. Zou, *ACS Energy Lett.* **2019**, *4*, 2975.
[105] G. Bounos, M. Karnachoriti, A. G. Kontos, C. C. Stoumpos, L. Tsetseris, A. Kaltzoglou, X. Guo, X. Lü, Y. S. Raptis, M. G. Kanatzidis, P. Falaras, *J. Phys. Chem. C* **2018**, *122*, 24004.
[106] M. W. Lufaso, P. M. Woodward, *Acta Crystallogr. Sect. B, Struct. Sci.* **2004**, *60*, 10.
[107] A. Jaffe, Y. Lin, W. L. Mao, H. I. Karunadasa, *J. Am. Chem. Soc.* **2015**, *137*, 1673.
[108] F. Aguado, F. Rodríguez, R. Valiente, J.-P. Itiè, M. Hanfland, *Phys. Rev. B* **2012**, *85*, 100101.
[109] Y. Moritomo, Y. Tokura, *J. Chem. Phys.* **1994**, *101*, 1763.
[110] Q. Li, S. Li, K. Wang, Z. Quan, Y. Meng, B. Zou, *J. Phys. Chem. Lett.* **2017**, *8*, 500.
[111] Y. Shi, Z. Ma, D. Zhao, Y. Chen, Y. Cao, K. Wang, G. Xiao, B. Zou, *J. Am. Chem. Soc.* **2019**, *141*, 6504.
[112] L. Zhang, C. Liu, Y. Lin, K. Wang, F. Ke, C. Liu, W. L. Mao, B. Zou, *J. Phys. Chem. Lett.* **2019**, *10*, 1676.
[113] Q. Li, L. Yin, Z. Chen, K. Deng, S. Luo, B. Zou, Z. Wang, J. Tang, Z. Quan, *Inorg. Chem.* **2019**, *58*, 1621.
[114] L. Zhang, C. Liu, L. Wang, C. Liu, K. Wang, B. Zou, *Angew. Chem., Int. Ed.* **2018**, *57*, 11213.
[115] L. Wu, Z. Dong, L. Zhang, C. Liu, K. Wang, B. Zou, *ChemSusChem* **2019**, *12*, 3971.
[116] L. Wang, P. Yao, F. Wang, S. Li, Y. Chen, T. Xia, E. Guo, K. Wang, B. Zou, H. Guo, *Adv. Sci.* **2020**, *7*, 1902900.
[117] D. B. Straus, S. Guo, R. J. Cava, *J. Am. Chem. Soc.* **2019**, *141*, 11435.
[118] J. A. Steele, H. Jin, I. Dovgaliuk, R. F. Berger, T. Braeckevelt, H. Yuan, C. Martin, E. Solano, K. Lejaeghere, S. M. J. Rogge, C. Notebaert, W. Vandezande, K. P. F. Janssen, B. Goderis, E. Debroye, Y.-K. Wang, Y. Dong, D. Ma, M. Saidaminov, H. Tan, Z. Lu, V. Dyadkin, D. Chernyshov, V. V. Speybroeck, E. H. Sargent, J. Hofkens, M. B. J. Roeffaers, *Science* **2019**, *365*, 679.
[119] G. Liu, J. Gong, L. Kong, R. D. Schaller, Q. Hu, Z. Liu, S. Yan, W. Yang, C. C. Stoumpos, M. G. Kanatzidis, H.-k. Mao, T. Xu, *Proc. Natl. Acad. Sci.* **2018**, *115*, 8076.
[120] S. Bonomi, I. Tredici, B. Albini, P. Galinetto, A. Rizzo, A. Listorti, U. Anselmi Tamburini, L. Malavasi, *Chem. Commun.* **2018**, *54*, 13212.
[121] O. V. Oyelade, O. K. Oyewole, D. O. Oyewole, S. A. Adeniji, R. Ichwani, D. M. Sanni, W. O. Soboyejo, *Sci. Rep.* **2020**, *10*, 7183.
[122] L. Shi, M. Zhang, Y. Cho, T. L. Young, D. Wang, H. Yi, J. Kim, S. Huang, A. W. Y. Ho-Baillie, *ACS Appl. Energy Mater.* **2019**, *2*, 2358.
[123] T. Luty, C. J. Eckhardt, *J. Am. Chem. Soc.* **1995**, *117*, 2441.
[124] M. C. Morón, F. Palacio, S. Clark, *Phys. Rev. B* **1996**, *54*, 7052.

Marta Morana is a postdoctoral fellow in the Material Chemistry Group at the Chemistry Department of the University of Pavia. Her main research interests are structural characterization of materials by means of single crystal and powder X-ray diffraction, structure–properties correlation, and crystallography at high pressure.

Lorenzo Malavasi is an associate professor at the Chemistry Department of the University of Pavia and member of the INSTM Consortium. Lorenzo's work deals with several areas of materials chemistry with particular interest in the investigation of structure–properties correlation in functional materials for sustainable and clean energy, in particular metal halide perovskites and catalysis materials. He leads the Materials Chemistry Group at University of Pavia.